Editors' Suggestion

Excitonic Interactions and Mechanism for Ultrafast Interlayer Photoexcited Response in van der Waals Heterostructures

Chen Hu,[1,2] Mit H. Naik,[1,2] Yang-Hao Chan,[1,2,3] and Steven G. Louie[1,2,*]
[1]Department of Physics, University of California at Berkeley, Berkeley, California 94720, USA
[2]Materials Sciences Division, Lawrence Berkeley National Laboratory, Berkeley, California 94720, USA
[3]Institute of Atomic and Molecular Sciences, Academia Sinica, and Physics Division, National Center for Theoretical Sciences, Taipei, 10617, Taiwan

(Received 30 May 2023; accepted 9 November 2023; published 8 December 2023)

Optical dynamics in van der Waals heterobilayers is of fundamental scientific and practical interest. Based on a time-dependent adiabatic *GW* approach, we discover a new many-electron (excitonic) channel for converting photoexcited intralayer to interlayer excitations and the associated ultrafast optical responses in heterobilayers, which is conceptually different from the conventional single-particle picture. We find strong electron-hole interactions drive the dynamics and enhance the pump-probe optical responses by an order of magnitude with a rise time of ∼300 fs in $MoSe_2/WSe_2$ heterobilayers, in agreement with experiment.

DOI: 10.1103/PhysRevLett.131.236904

By stacking a variety of two-dimensional (2D) material layers together, van der Waals (vdW) heterostructures offer a novel, versatile platform for exploring fascinating low-dimensional physics, such as Hofstadter butterfly states [1], topological phases [2,3], unconventional superconductors [4], and strong-correlated insulators [5]. Among the diverse 2D materials, the semiconducting monolayer transition metal dichalcogenide (TMD) family has attracted broad interest for photonics and optoelectronics because of their direct band gap properties and strong light-matter interactions [6]. Particularly, many TMD heterobilayers exhibit a type-II band alignment, i.e., the conduction band minimum (CBM) and the valence band maximum (VBM) reside in different layers. The type-II alignment provides a rich playground for investigating various optically induced exciton states (intralayer excitons on the individual layers and interlayer excitons across the two layers), as well as their dynamical evolution from mutual interactions [7–19].

Although recent optical pump-probe spectroscopies have provided rich experimental signatures on the ultrafast optical responses in heterobilayers [7–10], their accurate theoretical description and understanding remain to be fully understood. Most previous experimental interpretations on the interlayer optical dynamics are based on a "single-particle" picture: independent holes or electrons transfer from one monolayer to its neighbor through band hybridization or phonon-assisted scattering [7]. However, such an independent-particle (IP) picture is conceptually insufficient: in atomically thin TMD materials, the electrons and holes are known to be strongly bounded to form two-particle low energy states, i.e., excitons (correlated electron-hole pairs) with giant binding energy, due to enhanced Coulomb interaction from low-dimensional quantum confinement and reduced dielectric screening [6,20]. A vast literature of previous studies has shown that the IP picture cannot describe most optically induced phenomena even qualitatively in low-dimensional systems [20–26]. Therefore, a many-electron picture including electron-hole interactions (excitonic effects) is important to establish a more comprehensive interpretation of photoexcitation dynamics in TMD heterobilayers. However, this is significantly challenging in *ab initio* calculations because both time-dependent nonequilibrium dynamics and many-body excitonic physics need be accurately captured simultaneously.

In this study, going beyond the IP picture, we discover a *many-body excitonic mechanism*, as an alternative or additional channel, for the dynamics of converting photoexcited intralayer to interlayer excitations and for the associated ultrafast optical responses in TMD heterobilayers. We find that the couplings between the intralayer and interlayer excitonic states induce an ultrafast optical response, conceptually different from the direct single-particle charge transfer channel in the IP picture. Through our *ab initio* time-dependent calculations, strong excitonic effects are shown to play a crucial role on the ultrafast exciton dynamics and the pump-probe optical responses by enhancing the signal by over 1 order of magnitude with a rise time of about 300 fs. To investigate the real-time nonequilibrium dynamics including many-electron interactions and excitonic effects from first principles, we employ a recently developed *ab initio* time-dependent adiabatic *GW* approach (TD-a*GW*) [26] with real-time propagation of the density matrix in the presence of an external optical field.

In the TD-aGW framework [26],

$$i\hbar\frac{\partial}{dt}\rho_{nm,\boldsymbol{k}}(t) = [H^{aGW}(t), \rho(t)]_{nm,\boldsymbol{k}}, \tag{1}$$

where n and m are band indices, and $\rho_{nm,\boldsymbol{k}}(t)$ is the density matrix of the interacting many-electron system in the Bloch-state basis, which serves as the key quantity to explore the time-dependent field-driven nonequilibrium system. $H^{aGW}_{nm,\boldsymbol{k}}(t)$ is the TD-aGW Hamiltonian defined as

$$H^{aGW}_{nm,\boldsymbol{k}}(t) = h_{nm,\boldsymbol{k}} + U^{\text{ext}}_{nm,\boldsymbol{k}}(t) + \Delta V^{ee}_{nm,\boldsymbol{k}}(t). \tag{2}$$

Here, $h_{nm,\boldsymbol{k}}$ is the equilibrium quasiparticle Hamiltonian which includes all the equilibrium interactions (before photoexcitation) at the GW level, and it is independent of time. The external field part is given by $U^{\text{ext}}_{nm,\boldsymbol{k}}(t)$ which denotes the light-matter interaction and is equal to $-e\boldsymbol{E}(t)\cdot\boldsymbol{d}_{nm,\boldsymbol{k}}$, where $\boldsymbol{E}(t)$ is the optical electric field and $\boldsymbol{d}_{nm,\boldsymbol{k}}$ is the optical dipole matrix. Importantly, the photoinduced variation of the electron-electron interaction is given by $\Delta V^{ee}_{nm,\boldsymbol{k}}(t)$ which has two parts: $\Delta V^{ee}_{nm,\boldsymbol{k}}(t) = \Delta V^{H}_{nm,\boldsymbol{k}}(t) + \Delta\Sigma^{\text{COHSEX}}_{nm,\boldsymbol{k}}(t)$, where the first term is the Hartree potential and the second term is the nonlocal Coulomb hole plus screened-exchange (COHSEX) GW self-energy taken in the static screening limit which accounts for the time change of the many-electron (quasiparticle and excitonic) effects. In the TD-aGW approach, the excitonic effects is accurately captured at the GW plus Bethe-Salpeter equation (GW-BSE) level [26]. This is validated by the identical linear optical absorbance spectra (Fig. S2 in the Supplemental Material [27]) comparing results from standard GW-BSE calculations with those from TD-aGW. During the real-time evolution, we focus on the photoinduced time variation of the various quantities: $\Delta\rho(t) = \rho(t) - \rho(\text{eq.})$, $\Delta V^{ee}(t) = V^{ee}(t) - V^{ee}(\text{eq.})$, etc., where eq. denotes the equilibrium quantities (i.e., in the absence of a time-dependent driving external field). The formalism and computational details on the *ab initio* TD-aGW method can be found in the Supplemental Material [27].

Figures 1(a) and 1(b) illustrate the theoretical pump-probe setup. We focus on a representative and well-studied TMD heterobilayer—$MoSe_2/WSe_2$ with a common unit cell size of lattice constant 3.30 Å. As shown in Fig. 1(c), its quasiparticle band structure exhibits a type-II band alignment at the K point (as well as the K' point): the CBM (VBM) is mainly from the $MoSe_2$ (WSe_2) layer with a quasiparticle bandgap of 1.77 eV. There is very little layer hybridization for states near the K point, consistent with previous work [25]. Figure 2(a) shows the equilibrium linear optical absorbance of the system, which is computed by solving the GW-BSE (computational details are given in Supplemental Material [27]). Without electron-hole interactions, the IP picture fails to capture the main features seen in experiments (not shown) even qualitatively. On the other hand, the results with excitonic effects (red curve) show prominent absorption peaks corresponding to intralayer $MoSe_2$ excitons (electron and hole reside on the $MoSe_2$ layer), intralayer WSe_2 excitons (electron and hole reside on the WSe_2 layer), as well as interlayer excitons (electron and hole reside on the $MoSe_2$ and WSe_2, respectively), which have lower energies but weak optical response due to their small optical oscillator strengths.

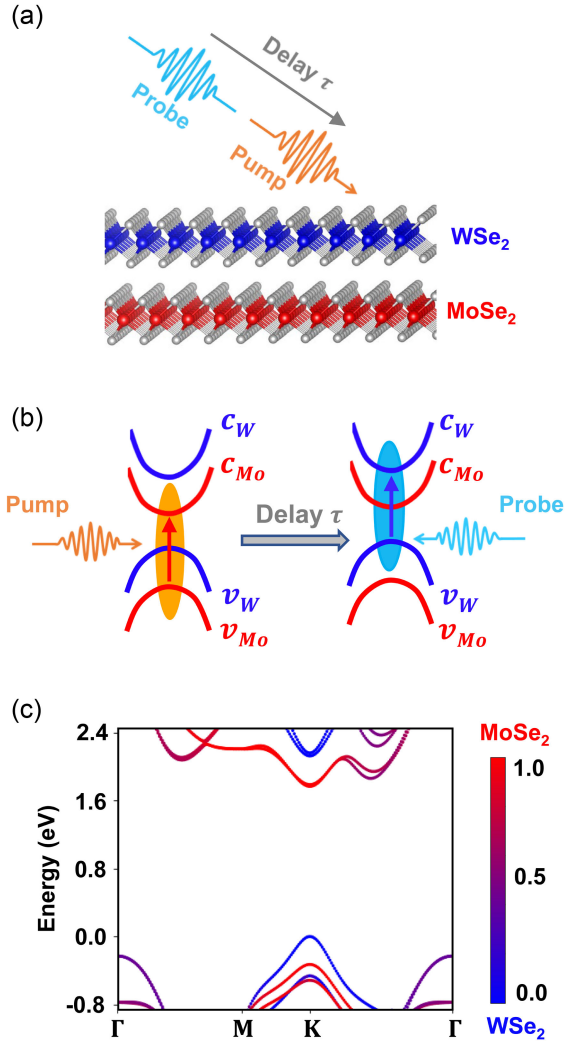

FIG. 1. (a)–(b) Schematic of the ultrafast optical pump-probe setup for study of $MoSe_2/WSe_2$ heterobilayers with a type II band alignment. The delay time τ denotes the time separation between the pump pulse and the probe pulse. Optically pumped excitation of 1s exciton in the $MoSe_2$ layer leads to the ultrafast interlayer dynamics which is probed by an optical pulse with WSe_2 1s exciton excitation energy after different time delay τ. c_W, c_{Mo}, v_W, v_{Mo} denote the conduction band of WSe_2 and $MoSe_2$, and the valence band of WSe_2 and $MoSe_2$, respectively. (c) GW quasiparticle band structure. The energy of the top of the valence band of the bilayer is set to be zero. The color represents the layer-component projection of each Bloch state to the different layers.

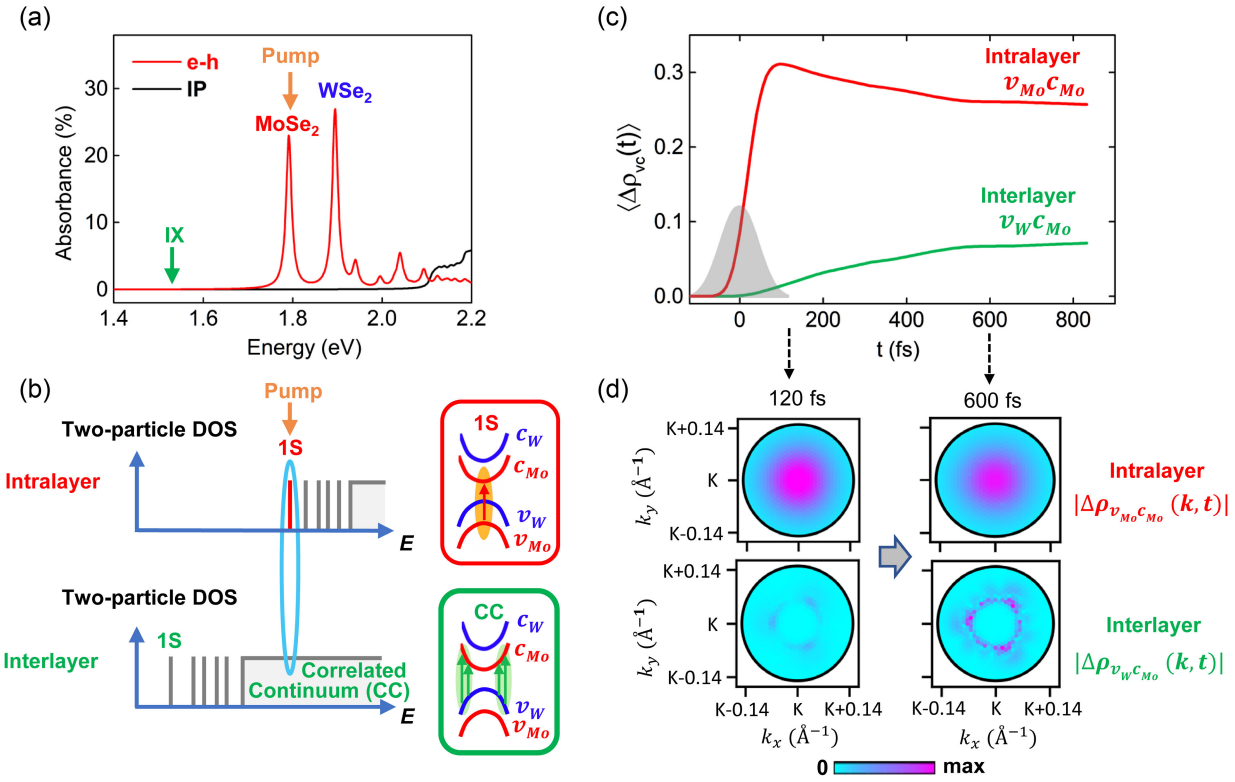

FIG. 2. (a) Optical absorbance of the $MoSe_2/WSe_2$ heterobilayer computed with (*e-h*, red solid line) and without (IP, black dashed line) electron-hole interactions. In both computations, quasiparticle self-energy corrections to the equilibrium band structure at the *GW* level are included. The position of the lowest-energy interlayer exciton (IX) is marked by the green arrow. (b) Schematic of coupling between intralayer ($MoSe_2$) 1*s* exciton and interlayer correlated-continuum (CC) excited states, indicated by the two-particle (correlated electron-hole pair) density of states (DOS). (c) Pump-induced real-time evolution of electron-hole coherence, as seen through an average of the photoinduced variations of the density matrix off diagonals: $\langle \Delta\rho_{vc}(t)\rangle = (1/N_k)\sum_{\boldsymbol{k}} |\Delta\rho_{vc,\boldsymbol{k}}(t)|^2$, where intralayer (red line) and interlayer (green line) quantities are given by taking $vc = v_{\mathrm{Mo}}c_{\mathrm{Mo}}$ and $v_W c_{\mathrm{Mo}}$, respectively. The gray shadow area shows the pump-pulse duration in time (Gaussian shape). We set the center of the pump pulse as zero of the time line. (d) *k*-space distributions of intralayer and interlayer electron-hole coherence magnitudes $|\Delta\rho_{vc}(\boldsymbol{k},t)|$ at two representative time points: snapshot at 120 and at 600 fs after the pump pulse, showing significant interlayer dynamics. In the plot, the distributions are shown around the *K* point.

Next, we investigate the real-time evolution of the interlayer and intralayer exciton states after the system is optically pumped at the $MoSe_2$ 1*s* exciton excitation energy [1.79 eV, the first peak in Fig. 2(a)], as shown in Fig. 1(b). In the IP picture, the main dynamics of the system would be that of independent carriers (e.g., photoinduced holes transferring from $MoSe_2$ layer to WSe_2 layer) through band hybridization or phonon-assisted scatterings. However, for 2D materials, the photoexcited holes are physically not "independent" but bound to the excited electrons forming correlated electron-hole pairs (excitons) with large binding energies (>300 meV). Therefore, as another channel for the dynamics going beyond the IP picture, we propose a new many-body excitonic picture as shown in Fig. 2(b): after pumping, the excited 1s exciton of $MoSe_2$ couples to the corelated-continuum (CC) states of the interlayer excited states which are in resonance in energy. Our TD-a*GW* calculations reveal that the dynamical coupling between the photoexcited $MoSe_2$ intralayer 1*s* exciton state and the interlayer excitonic continuum states in fact gives rise to a fast and significant time evolution in the system.

The computed real-time dynamics of an averaged photoinduced electron-hole coherence are shown in Figs. 2(c)–2(d). Here we define the averaged electron-hole coherence between two bands $\langle \Delta\rho_{vc}(t)\rangle$ from the change in the off-diagonals of the density matrix as $\langle \Delta\rho_{vc}(t)\rangle = (1/N_k)\sum_{\boldsymbol{k}} |\Delta\rho_{vc,\boldsymbol{k}}(t)|^2$. This quantity provides a measure of the correlation between the electrons and holes in the conduction band c and valence band v, respectively. As discussed below, the individual k-dependent $\Delta\rho_{vc,\boldsymbol{k}}(t)$ itself is of course the key quantity for determining the measured time-dependent optical responses. As shown in Fig. 2(c), after resonantly pumping at the $MoSe_2$ 1*s* exciton excitation energy (1.79 eV), the pump-induced $\langle \Delta\rho_{vc}(t)\rangle$ demonstrates two significant evolution dynamics: (i) During the pump-pulse duration [marked by the gray shadow in Fig. 2(c), with a full width at half maximum of 100 fs],

the intralayer $MoSe_2$ exciton is excited. The magnitude of $\Delta\rho_{v_{\mathrm{Mo}}c_{\mathrm{Mo}}}$ increases dramatically and reaches a maximum at the end of the pump pulse (at about 120 fs). In the upper left panel of Fig. 2(d), at $t = 120$ fs, a k-space distribution analysis reveals that the photoexcited intralayer $\Delta\rho_{v_{\mathrm{Mo}}c_{\mathrm{Mo}}}(\boldsymbol{k})$ is centered at the K point, showing typical $1s$ exciton features. The lower left panel of Fig. 2(d) indicates a very small interlayer $\Delta\rho_{v_W c_{\mathrm{Mo}}}(\boldsymbol{k})$. (ii) After the pump pulse ended (>120 fs), the magnitude of $\Delta\rho_{v_{\mathrm{Mo}}c_{\mathrm{Mo}}}$ shrinks with time along with a growth of the interlayer $\Delta\rho_{v_W c_{\mathrm{Mo}}}$, demonstrating the excited system is evolving rapidly from one of intralayer exciton character to one with increasing interlayer exciton character. Interestingly, as shown in the lower right panel of Fig. 2(d), the interlayer $\Delta\rho_{v_W c_{\mathrm{Mo}}}(\boldsymbol{k})$ is not concentrated at K point, reflecting a resonant coupling between the intralayer ($MoSe_2$) $1s$ exciton and interlayer correlated-continuum excited states as schematically indicated in Fig. 2(b). In general, for a two-level system, coupling between the two levels would lead to an oscillatory behavior in the real-time evolution, such as the oscillation dynamics between light and heavy hole excitons in semiconductor quantum well systems [43]. However, in the present case, the coupling is between the excited intralayer ($MoSe_2$) $1s$ exciton and a large set of continuum interlayer excitons with nearby energies [as shown in Fig. 2(b)] which gives rise to a smooth dynamics due to the interference of multiple oscillations.

We note that the coherence between holes in different layers ($\Delta\rho_{v_{\mathrm{Mo}}v_W}$) is significantly small, therefore a direct valence-to-valence band coupling is negligible, verifying that the single-particle picture of hole transition between valence bands of the two layers is not significant in the ultrafast timescale (Fig. S3 of the Supplemental Material [27]). Very fast phonon-assisted processes are needed if such mechanism is to be viable in the time regime of a few tens to hundreds of femtoseconds.

We now will discuss the driving forces that give rise to the dynamics. In the TD-aGW Hamiltonian [Eq. (2)], there are two time-dependent terms: the external field $U^{\mathrm{ext}}(t)$ and the internal electron-electron interaction $\Delta V^{ee}(t)$. The latter can be further spitted into two parts: $\Delta V^H(t)$ and $\Delta\Sigma^{\mathrm{COHSEX}}(t)$, as defined above. In Fig. 3, we compare the real-time evolution of the expectation values of these dynamical terms. Our *ab initio* results show that the $\Delta\Sigma^{\mathrm{COHSEX}}(t)$ term which accounts for the excitonic effects is dominant and much larger than the external field term and the Hartree term: the maximum magnitude ratios are $\langle\Delta\Sigma^{\mathrm{COHSEX}}\rangle/\langle\Delta V^H\rangle \approx 10$ and $\langle\Delta\Sigma^{\mathrm{COHSEX}}\rangle/\langle U^{\mathrm{ext}}\rangle \approx 30$, revealing the crucial role of strong excitonic effects. Therefore, excitonic effects are the dominant driving force and must be accurately included in the real-time evolution. Such Coulomb-mediated exciton dynamics is a general and fundamental mechanism which may also be important in other excitonic phenomena, such as exciton fission processes where a spin-singlet exciton transforms into two spin-triplet excitons [44,45].

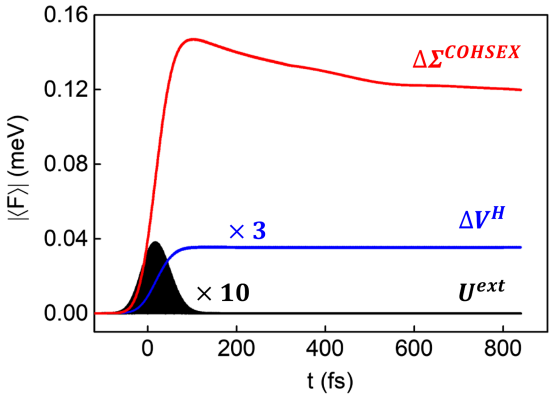

FIG. 3. Real-time evolution of various terms in the TD-aGW effective Hamiltonian. The expectation values of time dependence of different dynamical terms are defined as $\langle F(t)\rangle = \mathrm{Tr}\{\rho(t)F(t)\}$, where F is the external optical pump field (U^{ext}, black line), pump-induced Hartree potential variation (ΔV^H, blue line), or pump-induced many-body COHSEX self-energy variation ($\Delta\Sigma^{\mathrm{COHSEX}}$, red line).

In experiments, the ultrafast pump-induced intralayer-to-interlayer dynamical evolution of the system is measured by an optical pump-probe setup [8] as shown schematically in Fig. 1(b): a much weaker optical pulse is employed to probe one layer (e.g., WSe_2) after a time delay τ from a strong pump pulse on the other layer (e.g., $MoSe_2$), and the transient probe response signal is used to investigate the real-time system dynamics. Optically probing the interlayer excitation might offer another way to track the dynamics of interlayer excited states, but typically the very small oscillator strength of the interlayer transitions makes it experimentally impractical [as seen in the extremely weak computed interlayer optical response in Fig. 2(a)]. Instead, the WSe_2 $1s$ exciton [1.90 eV, the second peak in Fig. 2(a)] is optically probed in previous experiments after a pump pulse is used to excite the $MoSe_2$ $1s$ exciton [the first peak in Fig. 2(a)]. A widely measured quantity is the transient absorbance change $\Delta A/A$ defined as $[A_{\mathrm{pump\ on}}(\tau) - A_{\mathrm{pump\ off}}]/A_{\mathrm{pump\ off}}$, where $A_{\mathrm{pump\ on}}$ and $A_{\mathrm{pump\ off}}$ are optical absorbances at the probed energy after delay time τ, with and without the pump field [7–11], respectively. In our theoretical study, the transient optical properties are calculated from the polarization $\boldsymbol{P}(t) = (e/N_{\boldsymbol{k}}V)\sum_{nm,\boldsymbol{k}}\rho_{nm,\boldsymbol{k}}(t)\boldsymbol{d}_{mn,\boldsymbol{k}}$, where N_k is the number of k points in the BZ sampling and V is the volume of the unit cell. From this expression, it is clear that the optical dynamics is intrinsically related to the dynamics of $\rho_{nm,\boldsymbol{k}}(t)$ discussed above. The pump pulse induces a change in the polarizability and the band occupation corresponding to the off-diagonal and diagonal terms of $\rho_{nm,\boldsymbol{k}}(t)$, respectively, as well as in a change in the electron-electron interaction (as shown in Fig. 3). These effects contribute to

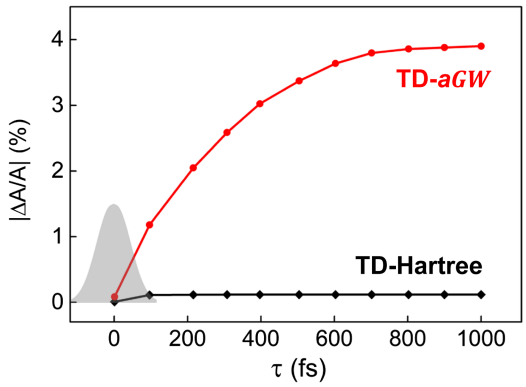

FIG. 4. Computed transient optical response as function of pump-probe delay time τ, as schematically depicted in Fig. 1(b). The black and red lines present the TD-aGW and TD-Hartree results, which are time evolutions with and without excitonic effects [i.e., many-body $\Delta\Sigma^{\mathrm{COHSEX}}(t)$ term] included, respectively. In both computations, quasiparticle self-energy corrections to the equilibrium band structure at the GW level are included. The gray shadow area shows the pump-pulse duration in time (Gaussian shape). In the theoretical pump-probe setup, the lowest-energy resonant excitations of $MoSe_2$ and WSe_2 from the different calculations are pumped and probed, respectively: in the TD-aGW (TD-Hartree) calculations, the pump and probe optical excitations are set as 1.79 (2.11) and 1.90 eV (2.19 eV), respectively.

the optical absorbance change in the pump-probe measurements. Our *ab initio* simulations here find that the dominant physics of the observed transient absorption change is from the dynamics of the off-diagonal terms of $\rho_{nm,\boldsymbol{k}}$ with n and m corresponding to bands localized on different layers. This may be understood qualitatively as a phase-space filling (PSF) effect, leading to a reduction in the amplitude for excitation of the WSe_2 intralayer exciton at a delayed time after pumping of the $MoSe_2$ intralayer exciton [46]. More details on the calculation of the transient optical absorbance from our *ab initio* TD-aGW method are given in the Supplemental Material [27].

As shown in Fig. 4, the computed transient absorbance change $\Delta A/A$ (in percents) from TD-aGW including excitonic effects exhibits a fast and prominent rise during and immediately after the pump duration (gray shadow in the plot). By fitting to an exponential form $c(1-e^{-\tau/t_r})$ we extract a theoretical rise time of $t_r \approx 300$ fs, which agrees well with the experimental measurements of about 200 fs at 9 K [8]. On the contrary, in the case of TD-Hartree calculation in which only the Hartree term $\Delta V^H(t)$ is included but ignoring excitonic effects from $\Delta\Sigma^{\mathrm{COHSEX}}(t)$, there is negligible change in the optical response with the pump pulse: the magnitude is about 30 times smaller than the full TD-aGW case and no discernable rising behavior exists after the pump pulse is subsided, which qualitatively disagree with experiments [8]. These results further evidence the key role of excitonic effects on the optical dynamics, which is consistent with the driving forces analysis in Fig. 3. In experiments, existing literature shows that difficult-to-control measurement deviations happen due to variations in relative layer orientation, sample quality, pump-probe details, and other technical issues, leading to a range for the value of the rise time from several tens of fs to hundreds of fs in various TMD heterobilayer samples [7–13]. Moreover, the effects of exciton-phonon coupling which lies outside of the scope of this Letter, is expected to bring additional scattering channels into the time evolution [14–19]. As a result, it may also contribute to the rise time which calls for future studies. The predicted hole transfer rate in $MoSe_2/WSe_2$ via a phonon-assisted process is computed to be approximately 400 fs at 300 K and exceeds 1000 fs at 100 K [15]; moreover, no significant temperature dependence was observed in the experiments [8].

In summary, we discover a new many-body excitonic channel for the ultrafast dynamics of photoinduced excited states and optical responses in TMD heterobilayers. Employing a recently developed *ab initio* TD-aGW method, we investigate the real-time evolution of the inter- and intralayer electron-hole coherence, and demonstrate that the couplings between the intralayer 1s exciton state and the interlayer correlated-continuum excited states in a $MoSe_2/WSe_2$ heterobilayer give rise to real-time excited-state and optical dynamics that are consistent with experiments. The strong excitonic effects in the van der Waals heterobilayers are shown as a major driving force for their excited-state dynamics and ultrafast pump-probe optical responses. The many-body excitonic picture, going beyond the independent-particle theory, thus provides new insights to the ultrafast optoelectronics in TMD heterostructures.

This work was supported by the Center for Computational Study of Excited-State Phenomena in Energy Materials (C2SEPEM) at LBNL, funded by the U.S. Department of Energy, Office of Science, Basic Energy Sciences, Materials Sciences and Engineering Division under Contract No. DE-AC02-05CH11231, as part of the Computational Materials Sciences Program which provided advanced codes and simulations, and supported by the Theory of Materials Program (KC2301) funded by the U.S. Department of Energy, Office of Science, Basic Energy Sciences, Materials Sciences and Engineering Division under Contract No. DE-AC02- 05CH11231, which provided conceptual and theoretical developments of exciton couplings. Y.-H. C. is supported by the National Science and Technology Council of Taiwan under Grant No. 112-2112-M-001-048. Computational resources were provided by the National Energy Research Scientific Computing Center (NERSC), which is supported by the Office of Science of the U.S. Department of Energy under Contract No. DE-AC02-05CH11231, Stampede2 at the Texas Advanced

Computing Center (TACC), The University of Texas at Austin through Extreme Science and Engineering Discovery Environment (XSEDE), which is supported by National Science Foundation under Grant No. ACI-1053575, and Frontera at TACC, which is supported by the National Science Foundation under Grant No. OAC-1818253. C. H. thanks Y. Yoon for fruitful discussions on pump-probe experiments, and Z. Li, M. Wu, J. Ruan, and J. Jiang for useful help on many-body theories and computations.

*sglouie@berkeley.edu

[1] B. Hunt *et al.*, Massive Dirac fermions and Hofstadter butterfly in a van der Waals heterostructure, Science **340**, 1427 (2013).

[2] Q. Tong, H. Yu, Q. Zhu, Y. Wang, X. Xu, and W. Yao, Topological mosaics in moire superlattices of van der Waals heterobilayers, Nat. Phys. **13**, 356 (2017).

[3] C. Hu, V. Michaud-Rioux, W. Yao, and H. Guo, Moiré valleytronics: realizing dense arrays of topological helical channels, Phys. Rev. Lett. **121**, 186403 (2018).

[4] Y. Cao, V. Fatemi, S. Fang, K. Watanabe, T. Taniguchi, E. Kaxiras, and P. Jarillo-Herrero, Unconventional superconductivity in magic-angle graphene superlattices, Nature (London) **556**, 43 (2018).

[5] Y. Cao *et al.*, Correlated insulator behaviour at half-filling in magic-angle graphene superlattices, Nature (London) **556**, 80 (2018).

[6] G. Wang, A. Chernikov, M. M. Glazov, T. F. Heinz, X. Marie, T. Amand, and B. Urbaszek, Colloquium: Excitons in atomically thin transition metal dichalcogenides, Rev. Mod. Phys. **90**, 021001 (2018).

[7] C. Jin, E. Y. Ma, O. Karni, E. C. Regan, F. Wang, and T. F. Heinz, Ultrafast dynamics in van der Waals heterostructures, Nat. Nanotechnol. **13**, 994 (2018).

[8] Z. Wang *et al.*, Phonon-mediated interlayer charge separation and recombination in a $MoSe_2/WSe_2$ heterostructure, Nano Lett. **21**, 2165 (2021).

[9] X. Hong, J. Kim, S.-F. Shi, Y. Zhang, C. Jin, Y. Sun, S. Tongay, J. Wu, Y. Zhang, and F. Wang, Ultrafast charge transfer in atomically thin MoS_2/WS_2 heterostructures, Nat. Nanotechnol. **9**, 682 (2014).

[10] H. Zhu, J. Wang, Z. Gong, Y. D. Kim, J. Hone, and X. Y. Zhu, Interfacial charge transfer circumventing momentum mismatch at two-dimensional van der Waals heterojunctions, Nano Lett. **17**, 3591 (2017).

[11] F. Ceballos, M. Z. Bellus, H.-Y. Chiu, and H. Zhao, Ultrafast charge separation and indirect exciton formation in a MoS_2-$MoSe_2$ van der Waals heterostructure, ACS Nano **8**, 12717 (2014).

[12] J. E. Zimmermann, M. Axt, F. Mooshammer, P. Nagler, C. Schüller, T. Korn, U. Höfer, and G. Mette, Ultrafast charge-transfer dynamics in twisted MoS_2/WSe_2 heterostructures, ACS Nano **15**, 14725 (2021).

[13] J. E. Zimmermann *et al.*, Directional ultrafast charge transfer in a $WSe_2/MoSe_2$ heterostructure selectively probed by time-resolved SHG imaging microscopy, Nanoscale Horiz. **5**, 1603 (2020).

[14] H. Wang, J. Bang, Y. Sun, L. Liang, D. West, V. Meunier, and S. Zhang, The role of collective motion in the ultrafast charge transfer in van der Waals heterostructures, Nat. Commun. **7**, 11504 (2016).

[15] Q. Zheng, Y. Xie, Z. Lan, O. V. Prezhdo, W. A. Saidi, and J. Zhao, Phonon-coupled ultrafast interlayer charge oscillation at van der Waals heterostructure interfaces, Phys. Rev. B **97**, 205417 (2018).

[16] Q. Zheng, W. A. Saidi, Y. Xie, Z. Lan, O. V. Prezhdo, H. Petek, and J. Zhao, Phonon-assisted ultrafast charge transfer at van der Waals heterostructure interface, Nano Lett. **17**, 6435 (2017).

[17] J. Zhang, H. Hong, C. Lian, W. Ma, X. Xu, X. Zhou, H. Fu, K. Liu, and S. Meng, Interlayer-state-coupling dependent ultrafast charge transfer in MoS_2/WS_2 bilayers, Adv. Sci. Lett. **4**, 1700086 (2017).

[18] Run Long and O. V. Prezhdo, Quantum coherence facilitates efficient charge separation at a $MoS_2/MoSe_2$ van der Waals junction, Nano Lett. **16**, 1996 (2016).

[19] J. Liu, X. Zhang, and G. Lu, Excitonic effect drives ultrafast dynamics in van der Waals heterostructures, Nano Lett. **20**, 4631 (2020).

[20] D. Y. Qiu, F. H. da Jornada, and S. G. Louie, Optical spectrum of MoS_2: Many-body effects and diversity of exciton states, Phys. Rev. Lett. **111**, 216805 (2013).

[21] D. Y. Qiu, F. H. da Jornada, and S. G. Louie, Environmental screening effects in 2D materials: Renormalization of the bandgap, electronic structure, and optical spectra of few-layer black phosphorus, Nano Lett. **17**, 4706 (2017).

[22] M. Wu, Z. Li, T. Cao, and S. G. Louie, Physical origin of giant excitonic and magnetooptical responses in two-dimensional ferromagnetic insulators, Nat. Commun. **10**, 2371 (2019).

[23] M. Wu, Z. Li, and S. G. Louie, Optical and magneto-optical properties of ferromagnetic monolayer CrBr: A first-principles GW and GW plus Bethe-Salpeter equation study, Phys. Rev. Mater. **6**, 014008 (2022).

[24] F. Zhang, C. S. Ong, J. Ruan, M. Wu, X. Q. Shi, Z. K. Tang, and S. G Louie, Intervalley excitonic hybridization, optical selection rules, and imperfect circular dichroism in monolayer h-BN, Phys. Rev. Lett. **128**, 047402 (2022).

[25] X. Lu, X. Li, and L. Yang, Modulated interlayer exciton properties in a two-dimensional moiré crystal, Phys. Rev. B **100**, 155416 (2019).

[26] Y.-H. Chan, D. Y. Qiu, F. H. da Jornada, and S. G. Louie, Giant exciton-enhanced shift currents and direct current conduction with subbandgap photo excitations produced by many-electron interactions, Proc. Natl. Acad. Sci. U.S.A. **118**, e1906938118 (2021).

[27] See Supplemental Material at http://link.aps.org/supplemental/10.1103/PhysRevLett.131.236904 for (i) computational details (DFT, *GW*-BSE and TD-a*GW*), (ii) geometric configuration of the $MoSe_2/WSe_2$ heterobilayer, (iii) comparison of optical absorbances computed from TD-a*GW* and *GW*-BSE, (iv) hole-hole coherence dynamics, and (v) calculated transient absorbance spectra, which includes Refs. [28–42].

[28] P. Giannozzi *et al.*, QUANTUM ESPRESSO: A modular and open-source software project for quantum simulations of materials, J. Phys. Condens. Matter **21**, 395502 (2009).

[29] M. S. Hybertsen and S. G. Louie, Electron correlation in semiconductors and insulators: Band gaps and quasiparticle energies, Phys. Rev. B **34**, 5390 (1986).
[30] M. Rohlfing and S. G. Louie, Electron-hole excitations in semiconductors and insulators, Phys. Rev. Lett. **81**, 2312 (1998).
[31] M. Rohlfing and S. G. Louie, Electron-hole excitations and optical spectra from first principles, Phys. Rev. B **62**, 4927 (2000).
[32] J. Deslippe, G. Samsonidze, D. A. Strubbe, M. Jain, M. L. Cohen, and S. G. Louie, BerkeleyGW: A massively parallel computer package for the calculation of the quasiparticle and optical properties of materials and nanostructures, Comput. Phys. Commun. **183**, 1269 (2012).
[33] D. R. Hamann, Optimized norm-conserving Vanderbilt pseudopotentials, Phys. Rev. B **88**, 085117 (2013).
[34] J. P. Perdew, K. Burke, and M. Ernzerhof, Generalized gradient approximation made simple, Phys. Rev. Lett. **77**, 3865 (1996).
[35] F. H. da Jornada, D. Y. Qiu, and S. G. Louie, Nonuniform sampling schemes of the Brillouin zone for many-electron perturbation-theory calculations in reduced dimensionality, Phys. Rev. B **95**, 035109 (2017).
[36] L. P. Kadanoff and G. Baym, *Quantum Statistical Mechanics* (W. A. Benjamin, Inc., New York, 1962).
[37] C. Attaccalite, M. Grüning, and A. Marini, Real-time approach to the optical properties of solids and nanostructures: Time-dependent Bethe-Salpeter equation, Phys. Rev. B **84**, 245110 (2011).
[38] L. Yang, J. Deslippe, C.-H. Park, M. L. Cohen, and S. G. Louie, Excitonic effects on the optical response of graphene and bilayer graphene, Phys. Rev. Lett. **103**, 186802 (2009).
[39] M. L. Cohen and S. G. Louie, *Fundamentals of Condensed Matter Physics* (Cambridge University Press, Cambridge, England, 2016).
[40] D. Sangalli, Excitons and carriers in transient absorption and time-resolved ARPES spectroscopy: An *ab initio* approach, Phys. Rev. Mater. **5**, 083803 (2021).
[41] D. Sangalli, S. Dal Conte, C. Manzoni, G. Cerullo, and A. Marini, Nonequilibrium optical properties in semiconductors from first principles: A combined theoretical and experimental study of bulk silicon, Phys. Rev. B **93**, 195205 (2016).
[42] E. Perfetto, D. Sangalli, A. Marini, and G. Stefanucci, Nonequilibrium Bethe-Salpeter equation for transient photoabsorption spectroscopy, Phys. Rev. B **92**, 205304 (2015).
[43] K. Leo, T. C. Damen, J. Shah, E. O. Gobel, and K. Köhler, Quantum beats of light hole and heavy hole excitons in quantum wells, Appl. Phys. Lett. **57**, 19 (1990).
[44] A. Rao and R. J. Friend, Harnessing singlet exciton fission to break the Shockley-Queisser limit, Nat. Rev. Mater. **2**, 17063 (2017).
[45] S. Refaely-Abramson, F. H. da Jornada, S. G. Louie, and J. B. Neaton, Origins of singlet fission in solid pentacene from an *ab initio* Green's function approach, Phys. Rev. Lett. **119**, 267401 (2017).
[46] S. Schmitt-Rink, D. S. Chemla, and D. A. B. Miller, Linear and nonlinear optical properties of semiconductor quantum wells, Adv. Phys. **38**, 89 (1989).